

A Novel Amino Lipid Series for mRNA Delivery: Improved Endosomal Escape and Sustained Pharmacology and Safety in Non-human Primates

Staci Sabnis,¹ E. Sathyajith Kumarasinghe,¹ Timothy Salerno,¹ Cosmin Mihai,¹ Tatiana Ketova,¹ Joseph J. Senn,¹ Andy Lynn,¹ Alex Bulychhev,¹ Iain McFadyen,¹ Joyce Chan,¹ Örn Almarsson,¹ Matthew G. Stanton,^{1,2} and Kerry E. Benenato¹

¹Moderna Therapeutics, 200 Technology Square, Cambridge, MA 02139, USA

The success of mRNA-based therapies depends on the availability of a safe and efficient delivery vehicle. Lipid nanoparticles have been identified as a viable option. However, there are concerns whether an acceptable tolerability profile for chronic dosing can be achieved. The efficiency and tolerability of lipid nanoparticles has been attributed to the amino lipid. Therefore, we developed a new series of amino lipids that address this concern. Clear structure-activity relationships were developed that resulted in a new amino lipid that affords efficient mRNA delivery in rodent and primate models with optimal pharmacokinetics. A 1-month toxicology evaluation in rat and non-human primate demonstrated no adverse events with the new lipid nanoparticle system. Mechanistic studies demonstrate that the improved efficiency can be attributed to increased endosomal escape. This effort has resulted in the first example of the ability to safely repeat dose mRNA-containing lipid nanoparticles in non-human primate at therapeutically relevant levels.

INTRODUCTION

mRNA-based therapies have the potential to revolutionize the way we treat diseases. The surging interest in mRNA as a drug modality stems from the potential to deliver transmembrane and intracellular proteins, targets that standard biologics are unable to access due to their inability to cross the cell membrane.¹ One major challenge to making mRNA-based therapies a reality is the identification of an optimal delivery vehicle. Due to its large size, chemical instability, and potential immunogenicity, mRNA requires a delivery vehicle that can offer protection from endo- and exo-nucleases, as well as shield the cargo from immune sentinels. Lipid nanoparticles (LNPs) have been identified as a leading option in this regard.² Moderna Therapeutics has recently validated this approach by demonstrating safe and effective delivery of an mRNA-based vaccine formulated in LNPs.³

Key performance criteria for an LNP delivery system are to maximize cellular uptake and enable efficient release of mRNA from the endosome. At the same time, the LNP must provide a stable drug product and be able to be dosed safely at therapeutically relevant levels. LNPs are multi-component systems that typically consist of an amino lipid,

phospholipid, cholesterol, and a PEG-lipid.² Each component is required for aspects of efficient delivery of the nucleic acid cargo and stability of the particle. The key component thought to drive cellular uptake, endosomal escape, and tolerability is the amino lipid. Cholesterol and the PEG-lipid contribute to the stability of the drug product both *in vivo* and on the shelf, while the phospholipid provides additional fusogenicity to the LNP, thus helping to drive endosomal escape and rendering the nucleic acid bioavailable in the cytosol of cells.

Several amino lipid series have been developed for oligonucleotide delivery over the past couple of decades.⁴ The literature highlights direct links between the structure of the amino lipid and the resultant delivery efficiency and tolerability of the LNP. The amino lipid MC3 (DLin-MC3-DMA) is the most clinically advanced oligonucleotide delivery system, as siRNA formulated in MC3-based LNPs has progressed to phase III for the treatment of transthyretin-mediated amyloidosis.^{5,6} More recently, literature reports have demonstrated the effectiveness of MC3-based LNPs to deliver mRNA.⁷ LNPs of this class are quickly opsonized by apolipoprotein E (ApoE) when delivered intravenously (*i.v.*), which enables cellular uptake into hepatocytes by the low-density lipoprotein receptor (LDLr).⁸ Concerns remain that MC3's long tissue half-life could contribute to unfavorable side effects hindering its use for chronic therapies.⁹ In addition, LNPs can induce activation of the immune system resulting in complement activation-related pseudoallergy (CARPA), an acute immunological response that can lead to anaphylactic-like shock.¹⁰

To unleash the potential of mRNA therapies for humans, we required a class of LNPs with increased delivery efficiency along with a metabolic and toxicity profile that would enable chronic dosing in humans.

Received 20 November 2017; accepted 9 March 2018;
<https://doi.org/10.1016/j.ymthe.2018.03.010>

²Present address: Generation Bio, 215 First Street, Suite 150, Cambridge, MA 02142, USA

Correspondence: Kerry E. Benenato, Moderna Therapeutics, 200 Technology Square, Cambridge, MA 02139, USA.

E-mail: kerry.benenato@modernatx.com



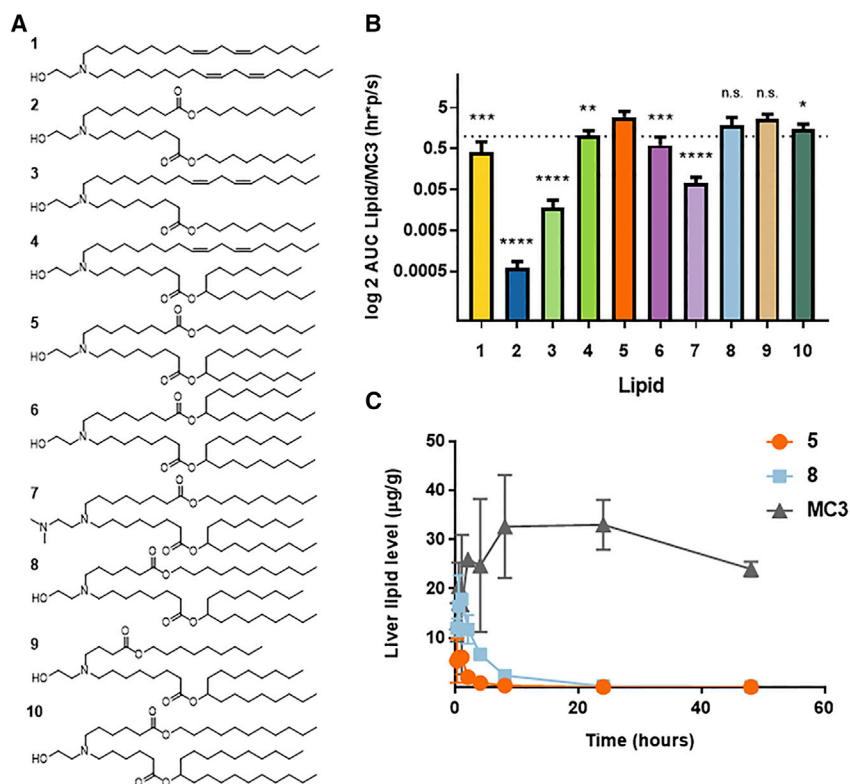


Figure 1. Optimization of Efficiency and Clearance of Amino Lipid

(A) Structures of amino lipids. (B) Whole-body luciferase bioluminescence AUC of novel LNPs versus MC3 LNPs, measured in CD-1 mice ($n = 6$ at 3 and 6 hr, $n = 3$ at 24 hr), 0.5 mg/kg dose firefly luciferase (fLuc) mRNA, i.v. bolus, error bars indicate SD of the ratio of novel lipid AUC versus MC3 AUC. * $p < 0.05$, ** $p < 0.01$, *** $p < 0.001$, **** $p < 0.0001$, n.s. = not statistically significant. (C) Parent amino lipid levels measured in liver tissue from Sprague-Dawley rats ($n = 3$ per time point), 0.2 mg/kg dose hEPO mRNA, mean \pm SD, $p < 0.05$ for lipids 5 and 8 AUC relative to MC3.

We took a rational medicinal chemistry approach to amino lipid optimization aiming to identify structural motifs that provide chemical stability, optimal tissue clearance, and mRNA delivery efficiency. Our initial rodent screens led to the identification of a lead lipid with good delivery efficiency and pharmacokinetics. The lead LNP was profiled further in non-human primate for efficiency of delivery after single and repeat dosing. Finally, the optimized LNPs were evaluated in 1-month repeat dose toxicity studies in rat and non-human primate.

RESULTS

Initial screening of a broad chemical space identified ethanolamine as an amino lipid head group that could effectively drive mRNA encapsulation and provide LNPs with superior physicochemical properties. Combining the ethanolamine head group with di-linoleic lipid tails (lipid 1; Figure 1; Table 1) generated an LNP with high encapsulation of luciferase mRNA, small particle size, and low polydispersity index (PDI). The LNP with lipid 1 had a surface pK_a (apparent value for the particle) in the range that has been shown to be optimal for siRNA delivery.^{11,12} To evaluate the efficiency of the new amino lipids, LNPs using the novel lipids were tested *in vivo* in mice using firefly luciferase mRNA as a reporter. An MC3 LNP was included as a control in each experiment, enabling us to compare LNPs from experiment to experiment. Measured luciferase activity also enabled us to determine protein bio-distribution. i.v. delivery of 0.5 mg/kg (mRNA dose level) of lipid 1-based LNPs to mice resulted in luciferase activity two-fold lower than an MC3 LNP control (Figure 1B).

Whole-body imaging clearly demonstrated that the majority of protein expression was localized in the liver (Figure S1). We found that the lipid had similar clearance to MC3 from liver tissue with 66% of the original dose remaining in liver tissue of mice 24 hr post-dose (Table 1).

To improve tissue clearance, we introduced ester linkages in the lipid tails (lipids 2 and 3; Figure 1A), which are reported to trigger metabolism by esterases *in vivo*.¹³ This has been shown to be a viable strategy to improve lipid clearance in a MC3-based lipid structure.⁹ First, we established that the lipids were chemically stable by measuring ethanol stability at room temperature and 37°C (Table S1). We observed less than 1% change in purity for all lipids tested. LNPs formed with lipid 2 were significantly larger with a surface $pK_a > 7$ (Table 1). Removal of one ester (lipid 3) afforded LNPs with improved physicochemical characteristics and lower LNP surface pK_a . *In vivo*, neither lipid demonstrated efficient mRNA delivery (Figure 1B); however, we did observe rapid tissue clearance, with no lipid detected at 24 hr (Table 1).

Improvement in protein expression was observed when a secondary ester was introduced (lipid 4; Figures 1A and 1B). We observed equivalent expression to MC3 LNPs, but the clearance rate was slower than lipids 2 and 3 (67% lipid remaining; Table 1). Replacement of the linoleic tail with a primary ester-containing lipid tail (lipid 5; Figure 1A) provided increased expression (3-fold higher than MC3; Figure 1B) and optimal tissue clearance (no lipid detected at 24 hr; Table 1). To further increase expression an additional secondary ester was introduced (6), but this resulted in a lowering of the surface pK_a to 6.00 and lower luciferase activity. In addition, the lipid had a significantly slower tissue clearance with 68% remaining at 24 hr.

With an optimal lipid tail structure identified we re-visited the ethanolamine head group. Lipid 7 is one representative example (Figure 1A) where the alcohol functionality is replaced with a dimethylamine. This generated an LNP with comparable physicochemical properties, but complete loss of delivery efficiency (Figure 1B).

Table 1. Lipid Nanoparticle Physicochemical Characterization and Lipid Tissue Clearance

Lipid	% EE ^a	Size (nm)	PDI ^b	pK _a	% Dose Remaining Mouse Liver Tissue, 24 hr ^c	% Dose Remaining Rat Liver Tissue, 48 hr ^d
1	96.9 ± 1.2	93.8 ± 5.6	0.14 ± 0.05	6.79 ± 0.37	66 ± 22	NT
2	91.8 ± 0.9	179.4 ± 4.2	0.14 ± 0.05	7.39 ± 0.07	0	NT
3	90.9 ± 0.9	140.4 ± 2.4	0.11 ± 0.05	6.95 ± 0.13	0	NT
4	97.6 ± 1.2	73.1 ± 2.1	0.07 ± 0.05	6.32 ± 0.05	67 ± 9.8	NT
5	97.5 ± 0.2	86.2 ± 1.7	0.04 ± 0.06	6.56 ± 0.13	0	0.02 ^e
6	97.0 ± 0.6	66.8 ± 1.1	0.11 ± 0.03	6.00 ± 0.24	68 ± 9.2	NT
7	95.2 ± 0.5	130.1 ± 3.5	0.15 ± 0.07	6.58 ± 0.11	NT	NT
8	95.8 ± 1.0	85.8 ± 1.0	0.10 ± 0.05	6.68 ± 0.29	NT	1.3 ^e
9	97.4 ± 0.2	91.9 ± 1.5	0.16 ± 0.03	6.64 ± 0.14	NT	20 ± 4.0 ^f
10	98.3 ± 0.2	69.6 ± 1.3	0.14 ± 0.04	6.77 ± 0.08	29 ± 2.9 ^f	NT
MC3	97.3 ± 1.9	85.6 ± 4.5	0.11 ± 0.04	6.30 ± 0.03	71 ± 27	61 ^e

NT = not tested, ±SD within one assay run.

^aPercent encapsulation efficiency.

^bPolydispersity index.

^cPercent of original lipid dose in CD-1 mouse liver 24 hr after 0.5 mg/kg i.v. bolus dose mRNA, n = 5 ± SD

^dPercent of original lipid dose in Sprague-Dawley rat liver 48 hr after 2 mg/kg i.v. bolus dose mRNA.

^en = 2.

^fn = 3 ± SD.

We further explored the lipid tail structure-activity relationship, specifically the position of the primary ester and how it affects delivery efficiency and tissue clearance (compare lipids 5, 8, and 9; [Figure 1A](#); [Table 1](#)). In mice, using luciferase mRNA, we observed higher expression compared to MC3 after i.v. delivery of a 0.5 mg/kg dose with lipids 8 and 9, with 9 providing the highest luciferase activity of the series ([Figure 1B](#)). Similar results were obtained in Sprague-Dawley rats using human erythropoietin (hEPO) encoding mRNA ([Figure S2](#)). When we determined the parent amino lipid levels in the liver at the termination of the rat study (48 hr post-dose), we observed the clearance was reduced as the primary ester was moved closer to the nitrogen (<1% 5, 1% 8, and 20% 9; [Table 1](#)). We found the effect on tissue clearance was more pronounced when we also modified the position of the secondary ester. With lipid 10, where both esters are located at the C6 position relative to the amine nitrogen ([Figure 1A](#)), we observed comparable luciferase activity in mice ([Figure 1B](#)); however, 29% of the original dose of the parent lipid remained in the liver tissue ([Table 1](#)). Based on the favorable rat data, we further progressed lipids 5 and 8 as they provided a good balance of delivery efficiency and pharmacokinetics.

To gain a better understanding of the lipid clearance profile, we performed a rat pharmacokinetic study that compared 5 and 8 to MC3 ([Figure 1C](#)). In contrast to MC3, which was still present at high concentrations at 48 hr, 5 and 8 were efficiently cleared from liver tissue by 24 hr. As shown in the previous experiment, 5 is cleared from the liver tissue faster than 8 with a liver tissue half-life of 5.8 hr versus 6.9 hr, respectively (for full PK parameters, see [Table S2](#)). This fast clearance is in sharp contrast to the >50 hr half-life of MC3. The favorable lipid degradation *in vivo* for 5 and 8 was also observed in spleen and plasma ([Table S2](#)).

Based on the measured tissue half-life of MC3, repeat dosing of mRNA in an MC3-based LNP for a therapeutic indication would be expected to lead to accumulation of the lipid in tissues. We therefore wanted to determine if the favorable single-dose pharmacokinetics of lipid 5 were maintained with weekly dosing. Clearance of MC3 and lipid 5 from multiple mouse tissues was measured after dosing 0.05 mg/kg mRNA on days 1, 8, and 15 ([Figure 2A](#)). Following dosing with MC3 LNPs, lipid was detected in liver, spleen, plasma, kidney, heart, and lung, with liver and spleen containing the largest concentrations ([Figure 2A](#); for full panel of tissues, see [Figure S3](#)). Accumulation of MC3 was observed after each dose. Liver and spleen had the highest levels of lipid 5, however, significantly lower levels than MC3. Lipid 5 was also detected in plasma, lung, and kidney, but not in heart ([Figure S3](#)). In terms of protein exposure with repeat dosing, we observed consistent levels of expression when 0.5 mg/kg hEPO mRNA was delivered i.v. to mice in lipid 5-based LNPs ([Figure 2B](#)), demonstrating the potential for repeat dosing.

To understand the clearance pathways involved, we also performed *in vitro* metabolite identification studies using lipid 5. These studies showed that, as expected, the initial step of metabolism of lipid 5 was primary ester hydrolysis to acid 11 ([Figure 2C](#); [Table S3](#)). Mimicking the previous repeat dose pharmacokinetic study, we measured the disappearance of parent lipid 5 and the primary metabolite 11 from mouse liver tissue after dosing 0.25 mg/kg mRNA on days 1, 8, and 15. As can be seen in [Figure 2D](#), we observed rapid clearance of both parent lipid 5 and metabolite 11.

While the above data illustrated improved delivery efficiency and pharmacokinetic properties (faster clearance) for this new series of ionizable lipids, we needed to translate the findings from rodent to

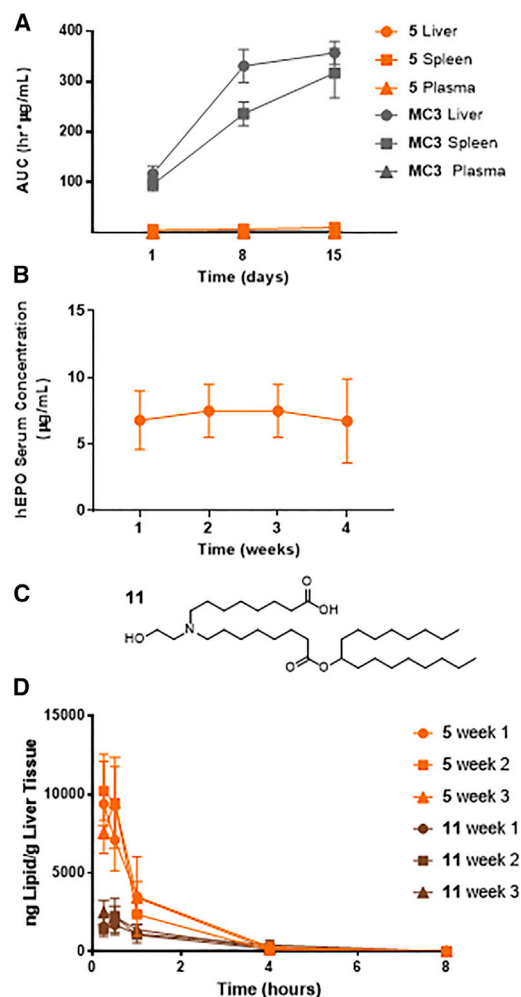


Figure 2. Pharmacokinetic and Expression Profile of Lipid 5 after Multiple Doses

(A) Comparison of tissue distribution of MC3 and lipid 5 after three i.v. bolus doses, CD-1 mice ($n = 3$ per time point, 1, 4, and 24 hr), 0.05 mg/kg mRNA, weekly dosing, mean \pm SD, lipid 5 AUC < MC3 AUC at $p < 0.05$ at all time points. (B) hEPO serum concentration, 6 hr, i.v. bolus, CD-1 mice ($n = 8$), 0.5 mg/kg dose mRNA, weekly dosing, mean \pm SD. (C) Structure of the primary metabolite (11) of lipid 5. (D) Liver tissue clearance of lipid 5 and metabolite 11, i.v. bolus, CD-1 mice ($n = 3$ per time point), 0.25 mg/kg dose mRNA, weekly dosing, mean \pm SD.

the non-human primate, which more closely approximates clinical responses for LNP-based systems.^{14,15} We therefore evaluated whether the improved expression observed in mouse and rat with LNPs containing lipid 5 could also be achieved in non-human primates after a single dose. Figure 3 shows results achieved with two different mRNA cargos. A dose of 0.01 mg/kg of hEPO encoding mRNA was delivered via a 60-min i.v. infusion. Relative to the MC3 LNP control, 5-fold higher exposure of hEPO protein was observed (Figure 3A). Similarly, using a second mRNA cargo encoding for an anti-human immunoglobulin G (IgG) influenza A antibody, a 5-fold increase in expression and a clear dose response was observed compared to an MC3 LNP (Figures 3B and S4). In a separate

study, we also evaluated the lipid tissue accumulation in non-human primates after a single dose. Consistent with results in rodents, MC3 residue was found in multiple tissues at 12 hr post-dose, with the highest levels being detected in liver and spleen. In contrast, lipid 5 was present at significantly lower levels (Figure S5). These preliminary data demonstrate translation of improved efficiency of delivery and rapid elimination of lipid 5 in non-human primates, which is a critical step toward clinical use of the lipid.

Critical to the advancement of mRNA-based therapies is the ability to safely chronically dose in humans. Toward this end, we evaluated the level of expression provided by the new LNPs in a repeat dose experiment in primate. A 0.2 mg/kg dose of hEPO mRNA in a lipid 5-based LNP was delivered via a 60-min i.v. infusion to cynomolgus monkeys ($n = 4$) once weekly for 5 weeks. As can be seen in Figure 3C, we observed consistent exposure over the course of the experiment, in line with our observations in rodent. This is the first example of the ability to chronically dose mRNA-containing LNPs in primates.¹⁶

Next, we evaluated whether the lipid 5-based LNPs demonstrated improved tolerability *in vivo*. A full toxicological evaluation of lipid 5-based LNPs in both Sprague-Dawley rat and cynomolgus monkey was performed using a standard 1-month study with weekly dosing at three dose levels in each species. In rat, we dosed at 0.05, 0.5, and 2 mg/kg and in non-human primate, we dosed at 0.1, 0.3, and 1 mg/kg. LNP-related toxicities associated with MC3-based LNP systems are generally associated with immunological (cytokine and complement activation) and hepatic injury. In the rat, there were no adverse findings with lipid 5. Figure 4 highlights the day 30 levels of alanine transferase (ALT; Figure 4A) and aspartate aminotransferase (AST; Figure 4B), two indicators of liver damage. There is minimal elevation of either enzyme at any dose level relative to PBS control, and this trend is consistent for all the clinical chemistry, hematology, and immunological markers measured. This is in sharp contrast to the toxicity profile of an MC3-based mRNA-containing LNP, where at a 0.3 mg/kg dose of mRNA, ALT and AST were elevated and pathology showed evidence of necrosis (Figure S6).¹⁶

Cynomolgus monkeys also showed minimal findings at all dose levels. Measurement of circulating mRNA levels after each dose demonstrated consistent exposures over the course of the experiment (Figure S7). Figure 4 highlights the ALT (Figure 4C) and AST (Figure 4D) levels for the 1 mg/kg dose where at day 30 the levels were at the same level as control. We observed minimal elevation in markers of immune activation including complement and cytokines. As can be seen in Figure 4E, no significant change was observed in C5b9 levels, the terminal complement activation product after dose 1 or dose 5. Figure 4F shows the slight variation above baseline observed for monocyte chemo-attractive protein (MCP-1).

In addition to profiling the pharmacokinetics and tolerability of the new lipid system, we were interested in understanding the

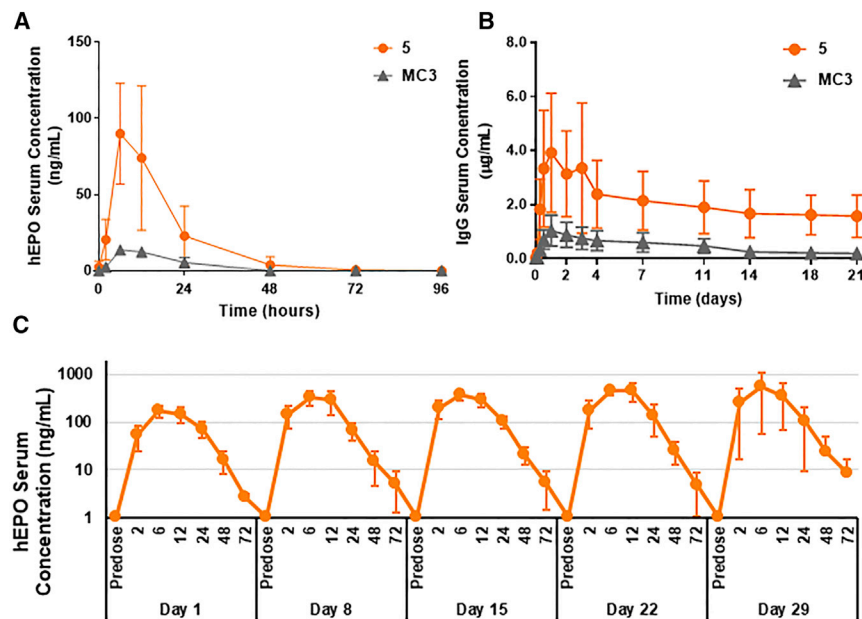


Figure 3. Expression Profile in Cynomolgus Monkey

(A) hEPO serum concentrations after delivery of 0.01 mg/kg hEPO mRNA in MC3 or lipid 5 LNPs, i.v. 60 min infusion, $n = 3$, mean \pm SD, $p < 0.05$ for lipid 5 AUC relative to MC3. (B) Human IgG influenza A antibody serum concentrations after delivery of 0.3 mg/kg antibody mRNA in MC3 or lipid 5 LNPs, i.v. 60 min infusion, $n = 3$, mean \pm SD, $p < 0.05$ for lipid 5 AUC relative to MC3. (C) hEPO serum concentrations after delivery of 0.2 mg/kg hEPO mRNA in lipid 5 LNPs, weekly dosing, i.v. 60 min infusion, $n = 4$, mean \pm SD.

(ratio of 0.76 and 0.13, respectively). Though with MC3, we observed higher LNP uptake into the cell (Figure 5B; Table 2), a higher percentage of lipid 5-based LNPs escape the endosome and deliver its mRNA to the cytosol due to higher fusogenicity. This conclusion is supported by the observation that lipid 5 has a lower onset T_m than MC3 (Table S5), a measurement which has been correlated with

increased fusogenicity and *in vitro* efficiency of siRNA containing LNPs.¹⁷

DISCUSSION

We found that multiple structural motifs of the amino lipid are important for efficient *in vivo* performance of mRNA-containing LNPs, including surface charge, structure, and position of the ester in the lipid tails and structure of the head group. In our work, we sought lipids that enabled high levels of protein expression, demonstrated rapid tissue clearance, and resulted in a toxicity profile that would support chronic therapeutic indications. Through optimization of the lipid tails, we observed variation of the surface pK_a of the particles, with the better LNPs having pK_a 's < 7 . However, being in the optimal pK_a range was not the only requirement for efficient delivery as dimethylamine lipid 7 demonstrated low levels of luciferase expression (Table 1). We found that introduction of a primary ester, similar to what has been observed with an MC3-based series,⁹ provided lipids which demonstrate rapid *in vivo* tissue clearance. Our metabolite identification studies with lipid 5 indicated that hydrolysis of the primary ester is the first step in the metabolism of the lipid. For this hydrolysis to be efficient, the sterics and electronics of the ester need to be balanced. More substituted esters (lipid 6) and lipids with the ester closer to the basic nitrogen (lipids 8, 9, and 10) each demonstrated slower liver clearance. The combination of the ethanolamine head group, a primary ester at the C8 position in one lipid tail, and a secondary ester in the second lipid tail provided the ideal balance of *in vivo* lipid clearance and protein expression.

Demonstration of cross-species translatability is required for the development of a new oligonucleotide delivery system. Through multiple expression and PK studies across species we were able to show similar profiles in mouse, rat, and nonhuman primate. i.v. delivery

underlying reason for the improved delivery efficiency relative to MC3, especially endosomal escape. Expression studies in ApoE knockout mice and LDLr knockout mice with lipid 5-based LNPs showed almost complete loss in expression, indicating that this amino lipid series has a similar uptake mechanism as MC3 and functions in an ApoE-mediated LDLr-dependent manner (Figure S8).⁸ To gain a better understanding of endosomal escape efficiency, we developed an *in vitro* cell-based assay using fluorescently labeled LNPs (incorporated 0.1% ATTO 647 DOPE to the LNP; magenta signal, Figures 5A and 5B). Single particle imaging on glass substrates (Figure 5A) was used to normalize cellular uptake and to derive the number of LNPs internalized at the single-cell level (Figure 5B; Table 2). To quantify cellular uptake, Stellaris single-molecule fluorescence *in situ* hybridization (smFISH; Quasar 570; red signal, Figure 5C) which detects both cytosolic mRNA and mRNA trapped in organelles was employed to detect total intracellular delivered mRNA. mRNA molecules that egressed the endocytic organelles into the cytosol were identified through object-based image analysis using the electroporated sample as benchmark for single mRNA intensity (Figure 5C, green). The selected single mRNA objects are pseudo-colored in green, overlaid over the smFISH signal (red). As can be seen in Figure 5, cells treated with lipid 5-based LNPs have a significantly lower amount of organelle aggregated mRNA (red) compared to cells treated with MC3-based LNPs (localization confirmed by co-staining with endosomal markers; Figure S12). At the same time, the density of single-molecule cytosolic mRNA objects (green) is higher in the lipid 5-based LNP-treated cells. To quantitatively compare the endosomal escape efficiency for the two LNP formulations, we computed the ratio between the number of cytosolic mRNA and the number of internalized LNPs at the single-cell level (Table 2). Our results show a 6-fold increase in efficiency for lipid 5 compared to MC3

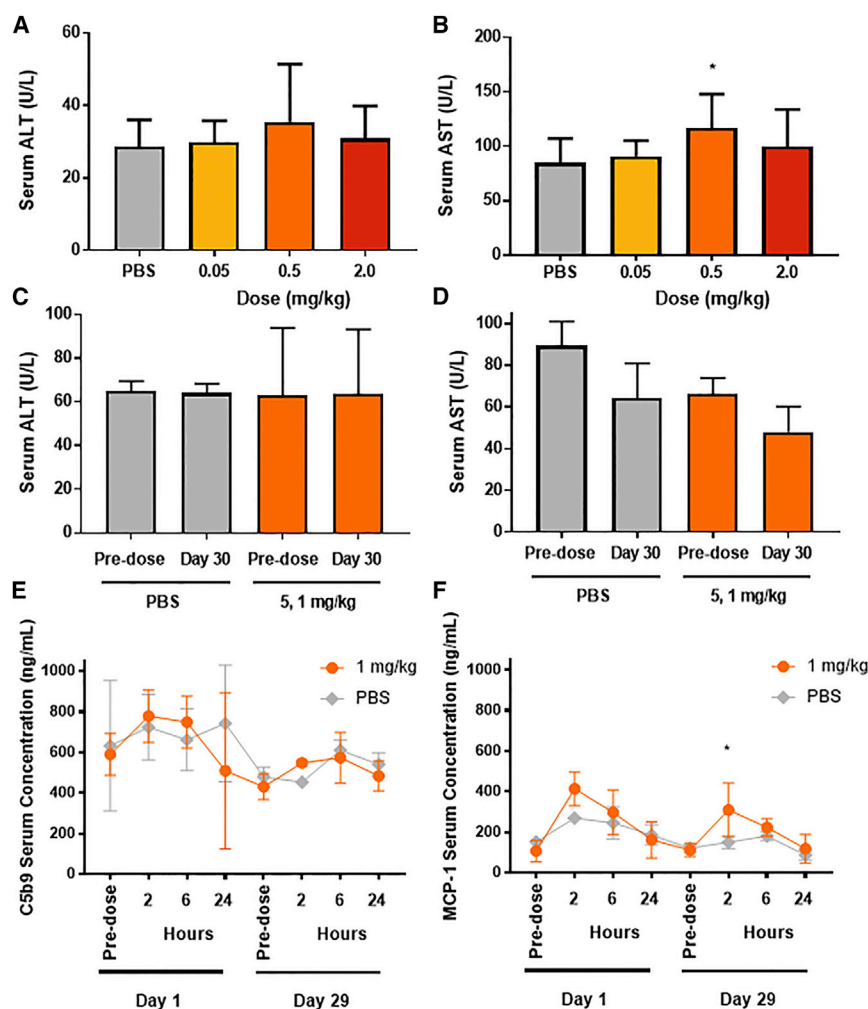


Figure 4. One-Month Toxicology Evaluation of Lipid 5 LNPs in Rat and Non-human Primate

(A) Serum alanine aminotransferase levels 24 hr post-fifth-dose, Sprague-Dawley rat, i.v. 10 min infusion, weekly dosing for 5 weeks, $n = 10$, mean \pm SD, no statistical difference between PBS and any dose level. (B) Serum aspartate aminotransferase levels 24 hr post-fifth-dose, Sprague-Dawley rat, i.v. 10 min infusion, weekly dosing for 5 weeks, $n = 10$, mean \pm SD, * $p < 0.05$, no statistical difference between PBS and 0.05 and 2.0 mg/kg dose. (C) Serum alanine aminotransferase levels 24 hr post-fifth-dose, cynomolgus monkey, 1 mg/kg mRNA, i.v. 60 min infusion, weekly dosing, $n = 4$, mean \pm SD, no statistical difference between PBS pre-dose and day 30 levels with lipid 5 levels. (D) Serum aspartate aminotransferase levels 24 hr post-fifth-dose, cynomolgus monkey, 1 mg/kg mRNA, i.v. 60 min infusion, weekly dosing, $n = 4$, mean \pm SD, no statistical difference between PBS pre-dose and day 30 levels with lipid 5 levels. (E) C5b9 serum concentration on day 1 and day 29, cynomolgus monkey, 1 mg/kg mRNA, i.v. 60 min infusion, weekly dosing, $n = 4$, mean \pm SD, no statistical difference between PBS and lipid 5 at all time points. (F) MCP-1 serum concentration on day 1 and day 29, cynomolgus monkey, 1 mg/kg mRNA, i.v. 60 min infusion, $n = 4$, mean \pm SD, * $p < 0.05$, no statistical difference between PBS and lipid 5 at any other time point.

taining LNPs with no evidence of toxicity and maintenance of circulating LNP levels.

Another key feature of the new delivery system is the improvement in endosomal escape. Gilleron et al.¹⁸ estimated that less than 2% of small interfering RNA (siRNA)-based LNPs that are taken up by the cell release their cargo into the cytosol. We were interested in prob-

ing this further to gain a better understanding of why our LNPs seem to be more efficient at endosomal escape relative to MC3. Using single-molecule fluorescence microscopy, we quantified endosomal escape efficiency (calculated as the ratio between number of cytosolic mRNA and number of internalized LNPs per cell) in an *in vitro* system, the first such report to our knowledge for LNP-mediated mRNA delivery. Our results show a 6-fold increase in efficiency for lipid 5 compared to MC3 (ratio of 0.76 and 0.13, respectively). Considering that these formulations encapsulate approximately five mRNA molecules per particle (see Figure S9 for method), the endosomal escape ratios reported here translate in 15% and 2.5% endosomal escape efficiency for lipid 5 and MC3, respectively, consistent with previous reports in the literature. It is of note that MC3 demonstrates higher *in vitro* uptake relative to lipid 5, however, this does not result in more mRNA being delivered to the cytosol. The endosomal escape process is driven by lipid fusogenicity and endosomal maturation as recently demonstrated by Heyes et al.¹⁷ and Patel and coworkers.¹⁹ We believe lipid 5-based LNPs are more fusogenic than MC3, resulting

of mRNA containing lipid 5-based LNPs in primate resulted in efficient expression of multiple proteins (Figures 3A, 3B, and S4) with similarly improved expression relative to MC3 as observed in rodent. In addition, the rapid clearance of lipid from tissue was also observed in non-human primates (Figure S5). Most importantly we were able to demonstrate efficient expression in non-human primates with lipid 5 LNPs over 5 weeks of dosing (Figure 3C).

Ideally, these novel ionizable lipids will allow for the safe and effective use of mRNA-based therapies in acute and chronic diseases. The optimization of the novel amino lipid series resulted in significant improvements in tolerability in rat and non-human primate as compared to MC3, which is in part due to the improved metabolic profile. Extensive literature evidence suggests that chronic dosing of LNPs can produce several toxic side effects, including CARPA and liver damage.¹⁰ In both rats and cynomolgus monkeys at doses up to 2 mg/kg and 1 mg/kg, respectively, we found no signals of liver damage or complement activation after 5 weeks of weekly dosing. These data provide the first evidence of repeat dosing of mRNA-con-

ing this further to gain a better understanding of why our LNPs seem to be more efficient at endosomal escape relative to MC3. Using single-molecule fluorescence microscopy, we quantified endosomal escape efficiency (calculated as the ratio between number of cytosolic mRNA and number of internalized LNPs per cell) in an *in vitro* system, the first such report to our knowledge for LNP-mediated mRNA delivery. Our results show a 6-fold increase in efficiency for lipid 5 compared to MC3 (ratio of 0.76 and 0.13, respectively). Considering that these formulations encapsulate approximately five mRNA molecules per particle (see Figure S9 for method), the endosomal escape ratios reported here translate in 15% and 2.5% endosomal escape efficiency for lipid 5 and MC3, respectively, consistent with previous reports in the literature. It is of note that MC3 demonstrates higher *in vitro* uptake relative to lipid 5, however, this does not result in more mRNA being delivered to the cytosol. The endosomal escape process is driven by lipid fusogenicity and endosomal maturation as recently demonstrated by Heyes et al.¹⁷ and Patel and coworkers.¹⁹ We believe lipid 5-based LNPs are more fusogenic than MC3, resulting

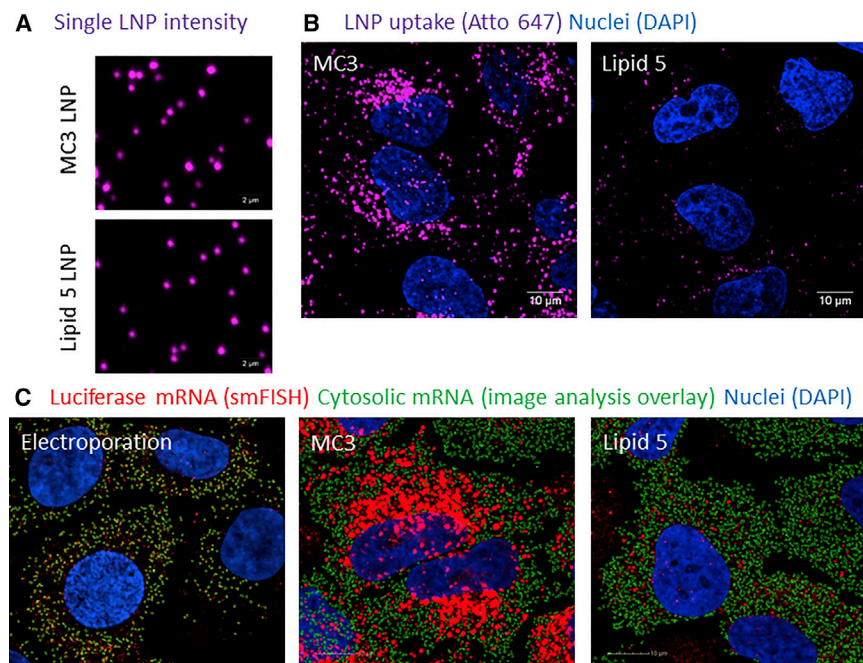


Figure 5. Fixed Cell Imaging of Endosomal Escape Efficiency

HeLa cells were transfected with ATTO 647 (magenta)-labeled MC3 and lipid 5 LNPs encapsulating luciferase mRNA, and processed for Stellaris single-molecule FISH (smFISH, Quasar 570, red) after 4 hr incubation, alongside cells electroporated with unformulated luciferase mRNA. The mRNA molecules that egressed the endocytic organelles into the cytosol are shown in green (image analysis overlay). Endosomal escape efficiency was evaluated by computing the ratio between the number of cytosolic mRNA (green) and the number of internalized LNPs per cell (magenta). (A) Single-particle imaging on glass, ATTO 647-labeled MC3, and lipid 5 LNPs (magenta). (B) ATTO 647-labeled LNP cellular uptake. (C) smFISH processing for intracellular delivered mRNA (red) and image analysis overlay (green).

increased endosomal escape and, therefore, a more efficient delivery vehicle.

The future of mRNA-based therapies relies on an efficient and safe delivery technology. The ability to treat a broad swath of diseases requires the flexibility to safely dose chronically at varying dose levels. Through systematic optimization of the amino lipid structure, we have identified lipids that balance chemical stability, improved efficiency of delivery due to improved endosomal escape, rapid *in vivo* metabolism, and a clean toxicity profile. The combination of these features provides a drug candidate that can be dosed chronically without activation of the immune system.

MATERIALS AND METHODS

mRNA Synthesis

Our mRNA was synthesized *in vitro* by T7 RNA polymerase-mediated transcription from a linearized DNA template, which incorporates the 5' and 3' untranslated regions (UTRs) and a poly(A) tail, as described in Richner et al.²⁰ The final mRNA utilizes Cap1 to increase mRNA translation efficiency. After purification, the mRNA is diluted in citrate buffer to the desired concentration.

Lipid Synthesis

Synthetic experimental details for all lipids can be found in the [Supplemental Materials and Methods](#).

Synthesis of heptadecan-9-yl 8-((2-hydroxyethyl)(8-(nonyloxy)-8-oxooctyl)amino)octanoate (5). To a solution of 8-bromooctanoic acid (5 g, 22 mmol) and nonan-1-ol (6.5 g, 45 mmol) in dichloromethane (100 mL) were added *N*-(3-dimethylaminopropyl)-*N'*-ethylcarbodi-

imide hydrochloride (4.3 g, 22 mmol) and 4-dimethylaminopyridine (DMAP) (547 mg, 4.5 mmol). The reaction was allowed to stir at room temperature for 18 hr. The reaction was diluted with dichloromethane and extracted with saturated NaHCO₃ (aqueous [a.q.]). The organic layer was separated and washed with brine, then dried over MgSO₄, filtered, and evaporated under vacuum. The residue was purified by silica gel chromatography (0%–10% ethyl acetate in hexanes) to obtain nonyl 8-bromooctanoate (6.1 g, 17 mmol, 77%). ¹H NMR (300 MHz, CDCl₃) δ: ppm 4.06 (triplet [t], 2H); 3.40 (t, 2H); 2.29 (t, 2H); 1.85 (multiplet [m], 2H); 1.72–0.97 (m, 22H); 0.88 (m, 3H).

A solution of nonyl 8-bromooctanoate (1.2 g, 3.4 mmol) and 2-aminoethan-1-ol (5 mL, 83 mmol) in ethanol (2 mL) was allowed to stir at 62°C for 18 hr. The reaction mixture was concentrated under vacuum, and the residue was extracted with ethyl acetate and water. The organic layer was separated and washed with water, brine, and dried over Na₂SO₄, then filtered and evaporated under vacuum. The residue was purified by silica gel chromatography (0%–100% [mixture of 1% NH₄OH, 20% MeOH in dichloromethane] in dichloromethane) to obtain nonyl 8-((2-hydroxyethyl)amino)octanoate (0.295 g, 26%). Ultra-performance liquid chromatography/evaporative light scattering detection (UPLC/ELSD): retention time (RT) = 1.29 min. Positive electrospray ionization mass spectrometry [MS (ES)]: *m/z* calculated for C₁₉H₄₀NO₅⁺ (mass plus one [M+H]), 330.53; found, 330.42. ¹H NMR (300 MHz, CDCl₃) δ: ppm 4.07 (t, 2H); 3.65 (t, 2H); 2.78 (t, 2H); 2.63 (t, 2H); 2.32–2.19 (m, 4H); 1.73–1.20 (m, 24H); 0.89 (m, 3H).

To a solution of 8-bromooctanoic acid (1.04 g, 4.6 mmol) and heptadecan-9-ol (1.5 g, 5.8 mmol) in dichloromethane (20 mL) were added *N*-(3-dimethylaminopropyl)-*N'*-ethylcarbodiimide hydrochloride (1.1 g, 5.8 mmol), *N,N*-diisopropylethylamine (3.3 mL, 19 mmol), and DMAP (0.11 g, 0.9 mmol). The reaction was allowed to stir at room temperature for 18 hr. The reaction was diluted with

Table 2. Endosomal Escape Efficiency

Condition	Number of Cytosolic mRNAs per Cell	Number of LNPs per Cell	Cytosolic mRNA/LNP
Electroporation	570 ± 19 ^a	NA	NA
MC3	550 ± 19 ^b	4230 ± 378 ^b	0.130
Lipid 5	717 ± 28 ^c	947 ± 71 ^c	0.758

NA = not applicable.

^aNumber of cells analyzed = 1,310.

^bNumber of cells analyzed = 1,439.

^cNumber of cells analyzed = 1,412.

dichloromethane and extracted with saturated NaHCO₃ (a.q.). The organic layer was separated and washed with brine, then dried over MgSO₄, filtered, and evaporated under vacuum. The residue was purified by silica gel chromatography (0%–10% ethyl acetate in hexanes) to obtain heptadecan-9-yl 8-bromooctanoate (875 mg, 41%). ¹H NMR (300 MHz, CDCl₃) δ: ppm 4.89 (m, 1H); 3.42 (m, 2H); 2.31 (m, 2H); 1.89 (m, 2H); 1.73–1.18 (broad [br.] m, 36H); 0.88 (t, 6H). ¹³C NMR (75 MHz, CDCl₃): δ 72.04, 37.51, 31.90, 29.73, 29.61, 29.29, 25.67, 22.68, 14.11.

A solution of nonyl 8-((2-hydroxyethyl)amino)octanoate (0.15 g, 0.42 mmol), heptadecan-9-yl 8-bromooctanoate (0.22 g, 0.47 mmol) and *N,N*-diisopropylethylamine (0.061 g, 0.47 mmol) in ethanol (2 mL) was allowed to stir at 65°C for 18 hr. The reaction was cooled to room temperature, and solvents were evaporated under vacuum. The residue was partitioned between ethyl acetate and saturated NaHCO₃ (aq.). The organic layer was separated, dried, and evaporated under vacuum. The residue was purified by silica gel chromatography (0%–100% [mixture of 1% NH₄OH, 20% MeOH in dichloromethane] in dichloromethane) to obtain heptadecan-9-yl 8-((2-hydroxyethyl)(8-(nonyloxy)-8-oxooctyl)amino)octanoate (0.089 g, 30%). UPLC/ELSD: RT = 3.59 min. High resolution electrospray ionization mass spectrometry [HRMS (ESI)]: *m/z* calculated for C₄₄H₈₈NO₅⁺ (M+H), 710.666; found, 710.659. ¹H NMR (300 MHz, CDCl₃) δ: ppm 4.86 (m, 1H); 4.05 (t, 2H); 3.53 (br. m, 2H); 2.83–2.36 (br. m, 5H); 2.29 (m, 4H); 1.71–1.41 (br. m, 13H); 1.40–1.17 (br. m, 51H); 0.88 (m, 9H). ¹³C NMR (75 MHz, CDCl₃): δ 173.81, 173.52, 74.03, 64.36, 58.31, 55.51, 53.82, 34.64, 34.30, 34.13, 31.84, 29.51, 29.48, 29.46, 29.23, 29.21, 29.15, 29.11, 28.64, 27.26, 27.23, 27.08, 25.91, 25.29, 25.09, 24.93, 22.64, 14.08.

Formulation

LNP formulations were prepared using a modified procedure of a method previously described for siRNA. In brief, lipids were dissolved in ethanol at molar ratios of 50:10:38.5:1.5 (ionizable lipid: DSPC: cholesterol:PEG-lipid). The lipid mixture was combined with a 6.25 mM sodium acetate buffer (pH 5) containing mRNA at a ratio of 3:1 (aqueous:ethanol) using a microfluidic mixer (Precision Nanosystems, Vancouver, BC). Formulations were dialyzed against PBS (pH 7.4) in dialysis cassettes for at least 18 hr. Formulations were concentrated using Amicon ultra centrifugal filters (EMD Millipore, Billerica, MA), passed through a 0.22-μm filter, and stored at 4°C un-

til use. All formulations were tested for particle size, RNA encapsulation, and endotoxin and were found to be between 80 nm–100 nm in size, with greater than 90% encapsulation and <1 EU/mL endotoxin.

TNS Assay

A master buffer stock was prepared (10 mM sodium phosphate, 10 mM sodium borate, 10 mM sodium citrate, 150 mM sodium chloride). This was used to prepare buffers at various pH values for determining apparent pK_a. Using 1 M sodium hydroxide and 1 M hydrochloric acid, 21 unique buffers from the master buffer stock were prepared at different pH values between about 3 and 12. Then a stock of 300 μM 6-(*p*-Toluidino)-2-naphthalenesulfonic acid sodium salt (TNS reagent) in DMSO was prepared. LNP was then prepared at a concentration of 0.04 mg/mL mRNA in the desired formulation buffer. This assay has been validated in 1 × PBS and 20 mM Tris with 8% sucrose buffer. Ninety microliters of each buffer was then added in triplicate to a black-bottomed 96-well plate (e.g., Costar 3916). To wells A1–A3, 90 μL of the lowest pH buffer solution was added. To wells B1–B3, 90 μL of the second lowest pH buffer solution was added. This process was repeated with all 21 pH buffer solutions. 3.26 μL of LNP sample at a concentration of 0.04 mg/mL mRNA was added to wells E7–E9. Two microliters of 300 μM TNS reagent solution was added to each well. Each well was then carefully mixed. Using a Synergy H1 plate reader, the plate was read. With the resulting fluorescence values, a sigmoidal plot of fluorescence versus buffer pH was created. The log of the inflection point of this curve was the apparent pK_a of the LNP formulation.

In Vivo Studies

Animals

Specific-pathogen-free female CD-1 female mice, 18–22 g in body weight, and male Sprague-Dawley rats, 225–250 g in body weight, were purchased from Charles River Laboratories (Kingston, New York). ApoE knockout (B6.129P2-Apoe^{Tm1Unc}/J; stock #002052), LDLr knockout (B6.129S7-Ldlr^{Tm1Her}/J; stock # 002207), and C57BL/6J mice (stock # 000664), all female mice, were purchased at 7 to 8 weeks of age from specific pathogen-free colonies at Jackson Laboratories (Bar Harbor, ME). All animals were housed in microisolator cages in a BSL-2 facility and provided water and food *ad libitum*. All research involving animals was conducted in accordance with Moderna Therapeutics' Animal Care and Use guidelines.

LNP Administration to Animals

mRNA-LNPs diluted in Dulbecco's PBS were injected i.v. (5 mL/kg) into mice or rats via the tail vein using 29 g, 3/10 cc insulin syringes (mice, BD Biosciences) or 27 g, 1 mL syringes (rats, BD Biosciences) after gentle warming of the animals using a heat lamp for 3 minutes.

Whole-Body and Ex Vivo Organ Bioluminescent Imaging of Mice Administered Luciferase mRNA

CD-1 mice were injected 15 min prior to the imaging time point intraperitoneally (i.p.) with 200 μL Xenolight D-luciferin K⁺ salt (catalog #122799; Perkin Elmer, Waltham, MA) diluted in PBS just prior to

use to a concentration of 15 mg/mL. Three minutes prior to imaging, mice were placed in an anesthesia-induction chamber filled with 3% isoflurane and 97% oxygen. Mice were moved into isoflurane-delivering nosecones in the imaging chamber (IVIS-Spectrum Model 124262; Perkin Elmer, Waltham, MA) immediately prior to imaging, positioned with ventral side up, and maintained on 3% isoflurane and 97% oxygen. Images were acquired using field of view D and continued to be exposed until 30,000 photons were collected or 1 min has passed, whichever occurred first. After whole-body imaging animals were returned to their home cage for recovery or were euthanized by CO₂ administration and organs removed for *ex vivo* imaging. In the latter case organs were placed on non-luminescent paper in the imaging chamber and images were acquired as detailed for whole body imaging. *Ex vivo* imaging of organs was completed within 25 min of luciferin administration. All images were quantified by region of interest for total flux using Living Image Software Version 4.4 (Perkin Elmer, Waltham, MA).

Blood Collection and Analysis for hEPO

Blood was collected from mice or rats via the tail vein, allowed to clot at room temperature in serum separator tubes (catalog #22-030-401; Fisher Scientific, Boston, MA). The tubes were then centrifuged at 7,000 rpm for 7 min and the sera samples aliquoted and stored at -80°C until analysis. hEPO concentrations were determined using a hEPO ELISA assay (catalog #01630; STEMCELL Technologies, Cambridge, MA) according to the manufacturer's instructions.

Non-human Primate Studies

Nonhuman primate studies were conducted at Charles River Laboratories (Sherbrooke, Quebec, Canada) using naive cynomolgus monkeys (*cynos*), 2–4 years old, weighing 2–6 kg. Animals were housed in stainless steel, perforated-floor cages, in a temperature- and humidity-controlled environment (21°C–26°C and 30%–70%, respectively), with an automatic 12-hr dark/light cycle. Animals were fed PMI Nutrition Certified Primate Chow No. 5048 twice daily. Tuberculin tests were carried out on arrival at the test facility. The study plan and procedures were approved by PCS-SHB IACUC. Animal experiments and husbandry followed NIH (NIH Publications No. 8023, 8th edition) and USA National Research Council and the Canadian Council on Animal Care (CCAC) guidelines. No treatment randomization or blinding methods were used for any of the animal studies. Sample sizes were determined by the resource equation method.

For injection, mRNA-LNPs in PBS (pH 7.2), were administered by 60-min i.v. infusion using a temporary indwelling catheter inserted in a peripheral vein.

hEPO ELISA for Non-human Primate Samples

Human Epo levels were measured using hEPO immunoassay from R&D Systems (catalog #DEP00) following manufacturer's recommendations. Cytokines levels were measured using non-human primate cytokine kit from Millipore (catalog #: PRCYTOMAG-40K) following manufacturer's recommendations.

Human IgG Analysis for Non-human Primate Samples

A 10.0 µL matrix aliquot was transferred to a low protein binding 96-well plate. A 25.0-µL aliquot of the working internal standard solution was added, and the sample aliquot was diluted with loading buffer. Human IgG and its internal standard were isolated using Protein A magnetic beads. After washing, the captured proteins were denatured using Rapigest, reduced using DTT, alkylated using iodoacetic acid, and digested with trypsin. The final extract was analyzed via HPLC with tandem mass spectrometry (MS/MS) detection using positive ion electrospray. A linear, 1/concentration² weighted, least-squares regression algorithm was used to quantitate unknown samples.

Serum ALT and AST Levels

Samples were analyzed using a Modular Analytics analyzer from Roche Diagnostics.

Serum C5b9 Levels

C5b9 sample analysis was performed using an ELISA method. The kit used was Human C5b-9 ELISA Set and Reagent Set B from BD Bioscience. Study samples were analyzed in singlicate diluted 1/100.

bdNA for Measurement of mRNA Levels

mRNA sample analysis (bdNA method) was performed using the QuantiGene 2.0 Reagent System kit from Affymetrix. Study samples were lysed prior to analysis using the QuantiGene Sample Processing Kit (blood samples). Study samples were analyzed in duplicate diluted between 1/100 and 1/1,250,000.

Quantification of Lipid by LC-MS/MS

Liver samples were homogenized by Omni probe following addition of 19 equivalent (eq.) (w/v) of water (dilution factor [DF] = 20), and protein was precipitated, and analyzed against calibration standards prepared in matching blank. Chromatographic separation and quantification was accomplished with a liquid chromatography (LC)-MS/MS system. Samples were injected and separated on Higgins Analytical Cliepus C8-column (Chrom Tech) equilibrated with 35% solvent A containing 5 mM formic acid 50% methanol (H₂O:MeOH:FA, 50:50:1) and 65% solvent B containing 5 mM formic acid in methanol (MeOH:FA 100:1, Thermo Fisher). A triple-quadrupole MS/MS system (Applied Biosystems, API 5500) operated in positive ion mode was used for signal detection.

Metabolite Identification

Human plasma from male and female donors containing K₂EDTA anticoagulant was obtained from Bioreclamation IVT (catalog #HMPLEDTA2; lot # BRH1140941). Lipid 5 (10 µM) was incubated with human plasma (29.0 mg protein/incubation) in incubation mixtures (200 µL final incubation volume) that consisted of 50/50 v/v neat plasma (undiluted)/substrate solution in 50 mM phosphate buffer (pH 7.4). Reactions were started by addition of the substrate solution to human plasma and were stopped at four designated time points (0, 30, 60, and 90 min) by the addition of 600 µL of stop reagent (acetonitrile). Stopped incubation samples

were centrifuged (e.g., $10,000 \times g$ for 10 min at 10°C), and the supernatant fractions were analyzed by LC-MS/MS to characterize the metabolites formed from lipid 5. Additional incubations were performed with the positive control procaine ($5 \mu\text{M}$) to establish competency of the test system. Samples were analyzed by LC-MS/MS with a quadrupole time-of-flight (QToF) mass spectrometer in positive mode with electrospray ionization for the acquisition of high-resolution accurate mass data. The experiment was executed on the Acquity UPLC system with in-line photodiode array detector equipped with Acquity BEH C18 ($100 \times 2.1 \text{ mm}$, $1.7 \mu\text{m}$) column and coupled with Xevo G2 XS instrument. Mobile phases used were 0.1% v/v formic acid in water and 0.1% v/v formic acid in acetonitrile.

Microscopy-Based Assay for Quantifying Endosomal Escape Efficiency

Fluorescently labeled LNPs (0.1% ATTO 647 DOPE) encapsulating Firefly Luciferase chemically modified *in vitro* transcribed mRNA (ATTO 647-Luc LNPs) were used to quantify LNP uptake, and single-molecule FISH (smFISH) allowed quantification of the number of cytosolic mRNA molecules. The complete workflow for deriving the endosomal escape efficiency is outlined in Figure S10. In brief, HeLa cells were plated in 96-well plates (Greiner BIO-ONE SensoPlate) using ATCC DMEM culture media, and upon reaching 80% confluency, the cells were incubated with cytoplasmic and nuclear detection labels (NucBlue Live, Blue CMAC, Thermo Fisher) per manufacturer protocols followed by transfection with ATTO 647-Luc LNPs at 50 ng (mRNA) per well in 100 μL volume. Cells were incubated with LNPs for 4 hr; after that the samples were fixed in 4% paraformaldehyde (Ted Pella) and imaged on the Opera Phenix spinning disk confocal (Perkin Elmer) using a $63\times$ water immersion objective (1.15 NA).

In parallel, cells were electroporated with unformulated luciferase mRNA using the Neon electroporation system (Thermo Fisher) with the manufacturer-recommended settings for HeLa cells. Electroporated cells were seeded in wells adjacent to the LNP-treated wells, and the entire plate was fixed at the same time. After the plate was imaged for LNP uptake, the samples were processed for smFISH hybridization (Stellaris Biosearch Technologies), using the manufacturer protocol. The plate was imaged on the Opera Phenix, and object analysis was used to quantify the number of single-molecule cytosolic mRNA (R, released from the endocytic organelles) in the LNP-treated samples using the electroporated samples as a benchmark (Figure S11). Co-staining with endocytic markers EEA1 (early endosomes) and Lamp1 (lysosomes) was used to confirm the intensity based analysis results (Figure S12).

ATTO 647-Luc LNPs were deposited directly on glass and imaged using the same acquisition settings used for the LNP-treated cells. The intracellular LNP uptake (number of LNPs per cell, L) was computed as the ratio between the fluorescence intensity sum per cell in the ATTO 647 channel (Cell_{Int}) and the average fluorescence intensity of single LNP objects on glass (LNP_{Int}). We used the endosomal

escape ratio (EER) defined as the ratio between the number of cytosolic mRNA and internalized LNPs (R/L) to compare the endosomal escape efficiency between the two formulations used in this study (5 and MC3).

Statistical Analysis

Means were compared using ordinary one-way ANOVA with post-hoc tests for multiple comparisons (Dunnett for comparing multiple conditions to a single reference or Sidák for comparing pairs of conditions). Areas under the curve (AUC) were calculated using the trapezoid rule and a z value calculated. For all tests, two-tailed p values < 0.05 were considered statistically significant, and are shown in the figures as * $p < 0.05$, ** $p < 0.005$, or *** $p < 0.001$. Prism 7.03 was used.

SUPPLEMENTAL INFORMATION

Supplemental Information includes Supplemental Materials and Methods, twelve figures, and four tables and can be found with this article online at <https://doi.org/10.1016/j.ymthe.2018.03.010>.

AUTHOR CONTRIBUTIONS

T.S., E.S.K., C.M., T.K., and J.C. ran experiments. I.M. performed statistical analysis. K.E.B., S.S., J.J.S., A.B., A.L., M.G.S., C.M., and Ö.A. designed experiments. K.E.B. wrote the manuscript.

CONFLICTS OF INTEREST

All authors own shares in Moderna Therapeutics.

ACKNOWLEDGMENTS

We would like to thank Lauren Knowles and the Moderna pharmacology department for execution of *in vivo* studies, Vikki Tsefrikas at Charles River Laboratories for bioanalysis support, and Kambiz Mousavi for contributions in the development of imaging assays.

REFERENCES

- Sahin, U., Karikó, K., and Türeci, Ö. (2014). mRNA-based therapeutics—developing a new class of drugs. *Nat. Rev. Drug Discov.* 13, 759–780.
- Haji, K.A., and Whitehead, K.A. (2017). Tools for translation: non-viral materials for therapeutic mRNA delivery. *Nat. Rev. Mater.* 2, 17056.
- Bahl, K., Senn, J.J., Yuzhakov, O., Bulychev, A., Brito, L.A., Hassett, K.J., Laska, M.E., Smith, M., Almarsson, Ö., Thompson, J., et al. (2017). Preclinical and clinical demonstration of immunogenicity by mRNA vaccines against H10N8 and H7N9 influenza viruses. *Mol. Ther.* 25, 1316–1327.
- Stanton, M.G., and Murphy-Beninato, K.E. (2017). Messenger RNA as a novel therapeutic approach. In *Topics in Medicinal Chemistry: RNA Therapeutics, Volume 27*, A. Garner, ed. (Springer), pp. 237–253.
- Coelho, T., Adams, D., Silva, A., Lozeron, P., Hawkins, P.N., Mant, T., Perez, J., Chiesa, J., Warrington, S., Tranter, E., et al. (2013). Safety and efficacy of RNAi therapy for transthyretin amyloidosis. *N. Engl. J. Med.* 369, 819–829.
- Butler, J.S., Chan, A., Costelha, S., Fishman, S., Willoughby, J.L.S., Borland, T.D., Milstein, S., Foster, D.J., Gonçalves, P., Chen, Q., et al. (2016). Preclinical evaluation of RNAi as a treatment for transthyretin-mediated amyloidosis. *Amyloid* 23, 109–118.
- Nabhan, J.F., Wood, K.M., Rao, V.P., Morin, J., Bhamidipaty, S., LaBranche, T.P., Gooch, R.L., Bozal, F., Bulawa, C.E., and Guild, B.C. (2016). Intrathecal delivery of frataxin mRNA encapsulated in lipid nanoparticles to dorsal root ganglia as a potential therapeutic for Friedreich's ataxia. *Sci. Rep.* 6, 20019.

8. Akinc, A., Querbes, W., De, S., Qin, J., Frank-Kamenetsky, M., Jayaprakash, K.N., Jayaraman, M., Rajeev, K.G., Cantley, W.L., Dorkin, J.R., et al. (2010). Targeted delivery of RNAi therapeutics with endogenous and exogenous ligand-based mechanisms. *Mol. Ther.* *18*, 1357–1364.
9. Maier, M.A., Jayaraman, M., Matsuda, S., Liu, J., Barros, S., Querbes, W., Tam, Y.K., Ansell, S.M., Kumar, V., Qin, J., et al. (2013). Biodegradable lipids enabling rapidly eliminated lipid nanoparticles for systemic delivery of RNAi therapeutics. *Mol. Ther.* *21*, 1570–1578.
10. Szebeni, J. (2014). Complement activation-related pseudoallergy: a stress reaction in blood triggered by nanomedicines and biologicals. *Mol. Immunol.* *61*, 163–173.
11. Semple, S.C., Akinc, A., Chen, J., Sandhu, A.P., Mui, B.L., Cho, C.K., Sah, D.W., Stebbing, D., Crosley, E.J., Yaworski, E., et al. (2010). Rational design of cationic lipids for siRNA delivery. *Nat. Biotechnol.* *28*, 172–176.
12. Jayaraman, M., Ansell, S.M., Mui, B.L., Tam, Y.K., Chen, J., Du, X., Butler, D., Eltepu, L., Matsuda, S., Narayanannair, J.K., et al. (2012). Maximizing the potency of siRNA lipid nanoparticles for hepatic gene silencing in vivo. *Angew. Chem. Int. Ed. Engl.* *51*, 8529–8533.
13. Fukami, T., and Yokoi, T. (2012). The emerging role of human esterases. *Drug Metab. Pharmacokinet.* *27*, 466–477.
14. Thess, A., Grund, S., Mui, B.L., Hope, M.J., Baumhof, P., Fotin-Mleczek, M., and Schlake, T. (2015). Sequence-engineered mRNA without chemical nucleoside modifications enables an effective protein therapy in large animals. *Mol. Ther.* *23*, 1456–1464.
15. DeRosa, F., Guild, B., Karve, S., Smith, L., Love, K., Dorkin, J.R., Kauffman, K.J., Zhang, J., Yabalom, B., Anderson, D.G., and Heartlein, M.W. (2016). Therapeutic efficacy in a hemophilia B model using a biosynthetic mRNA liver depot system. *Gene Ther.* *23*, 699–707.
16. Sedic, M., Senn, J.J., Lynn, A., Laska, M., Smith, M., Platz, S.J., Bolen, J., Hoge, S., Bulychev, A., Jacquinet, E., et al. (2018). Safety evaluation of lipid nanoparticle-formulated modified mRNA in the Sprague-Dawley rat and cynomolgus monkey. *Vet. Pathol.* *55*, 341–354.
17. Heyes, J., Palmer, L., Bremner, K., and MacLachlan, I. (2005). Cationic lipid saturation influences intracellular delivery of encapsulated nucleic acids. *J. Control. Release* *107*, 276–287.
18. Gilleron, J., Querbes, W., Zeigerer, A., Borodovsky, A., Marsico, G., Schubert, U., Manygoats, K., Seifert, S., Andree, C., Stöter, M., et al. (2013). Image-based analysis of lipid nanoparticle-mediated siRNA delivery, intracellular trafficking and endosomal escape. *Nat. Biotechnol.* *31*, 638–646.
19. Patel, S., Ashwanikumar, N., Robinson, E., DuRoss, A., Sun, C., Murphy-Beninato, K.E., Mihai, C., Almarsson, Ö., and Sahay, G. (2017). Boosting intracellular delivery of lipid nanoparticle-encapsulated mRNA. *Nano Lett.* *17*, 5711–5718.
20. Richner, J.M., Himansu, S., Dowd, K.A., Butler, S.L., Salazar, V., Fox, J.M., Julander, J.G., Tang, W.W., Shresta, S., Pierson, T.C., et al. (2017). Modified mRNA vaccines protect against Zika virus infection. *Cell* *168*, 1114–1125.e10.